Int. J. Solids Structures Vol. 30, No. 8, pp. 1093–1112, 1993
Printed in Great Britain

0020–7683/93 $6.00+ .00

A VARIABLE STIFFNESS TYPE ELASTOPLASTIC BOUNDARY ELEMENT FORMULATION FOR PLANAR ANISOTROPIC MEDIA

A. DEB and P. K. BANERJEE
Department of Civil Engineering, State University of New York at Buffalo,
240 Ketter Hall, Buffalo, NY 14260, U.S.A.

(*Received* 16 *December* 1991; *in revised form* 10 *August* 1992)

Abstract—An initial-stress boundary element algorithm has been presented for two-dimensional anisotropic elastoplasticity. A quadratic stress yield criterion with strain hardening recently derived and applied to Boron–Aluminum composites is adopted. The details relating to numerical evaluation of singular surface and volume integrals are discussed. A new generation iterative Newton–Raphson algorithm has been adopted to solve the nonlinear boundary element equations. The validity of the present formulation has been established with the help of examples.

INTRODUCTION

The boundary element method is recognized as an accurate numerical approach for a multitude of problems in physical sciences and engineering. Historically, the method which is based on singular boundary integral equations was conceived as a general tool for solving linear problems only. However the visualization of nonlinear problems as state dependent "incrementally linear" and "pseudo-body force" problems has made possible the extension of the method to the nonlinear zone.

The present paper deals with the type of nonlinearity that arises from elastoplastic constitutive modeling of anisotropic materials particularly advanced fiber reinforced composites. The boundary element method has already been successfully applied to a large class of elastoplastic problems that are initially isotropic (Riccardella, 1973; Banerjee *et al.*, 1979, 1989; Cathie and Banerjee, 1980; Mukherjee, 1982; Banerjee and Raveendra, 1986, 1987; Henry and Banerjee, 1987, 1988; Chopra and Dargush, 1992). Cruse and Polch (1986a, b) described a simple iterative initial-strain elastoplastic boundary element formulation intended to be used for local inelastic deformation analyses of anisotropic materials. However, the latter authors restricted their implementation to von Mises' criterion applicable to isotropic materials only and used flat boundary elements. Moreover, their simple iterative algorithm is not applicable to problems involving significant inelastic deformation. In the present work, a realistic constitutive model is chosen to describe the elastoplastic behavior of orthotropic composites with strain hardening. Yielding according to this model is governed by a quadratic stress criterion and has been the subject of discussion recently (Kenaga *et al.*, 1987). The solution of the nonlinear equations derived here using an initial-stress based variable stiffness type approach closely follows the iterative Newton–Raphson type of approach applied by Chopra and Dargush (1992) for isotropic thermo-plastic problems. The present formulation can also account for common body force loadings such as inertial and centrifugal forces (Deb and Banerjee, 1990) without resorting to additional volume integrals. The development of the nonlinear procedure is presented systematically and is followed by a comprehensive discussion of the iterative algorithm that is validated with an example.

ELASTIC CONSTITUTIVE RELATION

The elastic relation for an anisotropic material with a degree of anisotropy not greater than monoclinic can be written as

$$\begin{Bmatrix} \varepsilon_1 \\ \varepsilon_2 \\ \varepsilon_6 \end{Bmatrix} = \begin{bmatrix} b_{11} & b_{12} & b_{16} \\ & b_{22} & b_{26} \\ & \text{symmetric} & b_{66} \end{bmatrix} \begin{Bmatrix} \sigma_1 \\ \sigma_2 \\ \sigma_6 \end{Bmatrix} \tag{1}$$

or, in a symbolic form

$$\varepsilon_i = b_{ij}\sigma_j \quad (i, j = 1, 2, 6), \tag{1a}$$

where, ε_1 and ε_2 are normal strains in the x_1 and x_2 directions, respectively, and ε_6 is the shear strain in the x_1–x_2 plane, the values of σ_i are the corresponding Cauchy stresses, and b_{ij} represent material compliance coefficients.

It may be noted that for orthotropic materials, the elastic compliances can be expressed in terms of physically meaningful principal moduli E_1 and E_2, Poisson's ratio ν_{21} (or, ν_{12}) and in-plane shear modulus G_{12} as follows:

$$b_{11} = \frac{1}{E_1}, \quad b_{12} = -\frac{\nu_{21}}{E_2} = -\frac{\nu_{12}}{E_1}, \quad b_{16} = b_{26} = 0, \quad b_{22} = \frac{1}{E_2}, \quad b_{66} = \frac{1}{G_{12}}.$$

The inverse of relation (1) expressed as

$$\sigma_i = c_{ij}\varepsilon_j \quad (i, j = 1, 2, 6) \tag{2}$$

is also useful. Here, c_{ij} represents reduced stiffness coefficients for plane stress.

QUADRATIC STRESS YIELD CRITERION

A special case of the Tsai–Wu (1971) yield criterion, termed as the quadratic stress yield criterion applicable to orthotropic materials, together with isotropic strain hardening has been used by Kenaga *et al.* (1987) for characterizing a Boron–Aluminum composite. This criterion may be stated as follows for the case of plane stress:

$$f(\sigma_i) = f'(\sigma_i') = F_{11}\sigma_1'^2 + F_{22}\sigma_2'^2 + 2F_{12}\sigma_1'\sigma_2' + 2F_{66}\sigma_6'^2 = k(\varepsilon_{eq}^p), \tag{3}$$

where σ_i' denotes stress components referred to the material principal axes (Fig. 1) and σ_i to the global or geometric axes. The quantity k on the right-hand side of eqn (3) is a function of the equivalent plastic strain ε_{eq}^p and determines the progression of the stress surface beyond first yield.

It is noted that to obtain von Mises' yield criterion from eqn (3) the following substitutions are necessary:

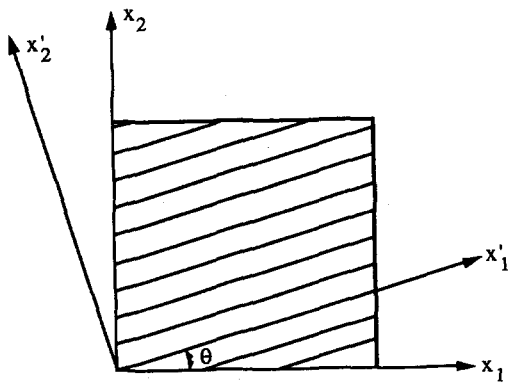

Fig. 1. Orientation of principal material axes (x_1'–x_2') of an orthotropic material.

$$F_{11} = F_{22} = \tfrac{2}{3}, \quad F_{12} = -\tfrac{1}{3}, \quad F_{66} = 1, \quad k = \tfrac{2}{3}\sigma_y^2,$$

where σ_y is the uniaxial yield stress for an isotropic material.

ELASTO-PLASTIC CONSTITUTIVE RELATION

The derivation of the elasto-plastic constitutive relation between the incremental stresses and strains is carried out as outlined below employing the yield criterion given by (3) together with a hardening rule and an associated flow rule.

We have from eqn (3) the following consistency condition:

$$\mathrm{d}f = \frac{\partial f}{\partial \sigma_i}\dot{\sigma}_i - \frac{\partial k}{\partial \varepsilon_{eq}^p}\dot{\varepsilon}_{eq}^p = 0. \tag{4}$$

Equivalent stress σ_{eq} is defined as

$$\sigma_{eq} = \sqrt{\tfrac{3}{2}f(\sigma_i)} = \sqrt{\tfrac{3}{2}f'(\sigma_i')}. \tag{5}$$

The work equivalent plastic strain increment $\dot{\varepsilon}_{eq}^p$ is obtained using incremental plastic work $\dot{W}_p$ in the following form:

$$\dot{W}_p = \sigma_i \dot{\varepsilon}_i^p = \sigma_{eq}\dot{\varepsilon}_{eq}^p \quad (i = 1, 2, 6), \tag{6}$$

whence

$$\dot{\varepsilon}_{eq}^p = \frac{\sigma_i \dot{\varepsilon}_i^p}{\sigma_{eq}}. \tag{7}$$

As per the associated flow rule (also called the normality condition), we have

$$\dot{\varepsilon}_i^p = \dot{\lambda}\frac{\partial f}{\partial \sigma_i} \quad (i = 1, 2, 6), \tag{8}$$

where $\dot{\lambda}$ is a scalar factor of proportionality.

From the last two equations we have

$$\dot{\varepsilon}_{eq}^p = \frac{\dot{\lambda}}{\sigma_{eq}}\sigma_i \frac{\partial f}{\partial \sigma_i}. \tag{9}$$

Let us define the following notation:

$$\bar{\boldsymbol{\sigma}} = \{\sigma_1 \quad \sigma_2 \quad \sigma_6\}^T, \tag{10a}$$

$$\frac{\partial f}{\partial \bar{\boldsymbol{\sigma}}} = \left\{\frac{\partial f}{\partial \sigma_1} \quad \frac{\partial f}{\partial \sigma_2} \quad \frac{\partial f}{\partial \sigma_6}\right\}^T. \tag{10b}$$

The transformation of stresses between the global and the material principal axes is defined as follows:

$$\bar{\boldsymbol{\sigma}}' = \mathbf{T}\bar{\boldsymbol{\sigma}}, \tag{11}$$

where the transformation matrix denoted by $\mathbf{T}$ is given in the Appendix. It can be shown that the derivatives of the yield surface transform as follows:

$$\frac{\partial f}{\partial \bar{\sigma}} = \mathbf{T}^{\mathrm{T}} \frac{\partial f'}{\partial \bar{\sigma}'}. \tag{12}$$

Now,

$$\sigma_i \frac{\partial f}{\partial \sigma_i} = \left(\frac{\partial f}{\partial \bar{\sigma}}\right)^{\mathrm{T}} \bar{\sigma} = \left(\mathbf{T}^{\mathrm{T}} \frac{\partial f}{\partial \bar{\sigma}}\right)^{\mathrm{T}} (\mathbf{T}^{-1}\bar{\sigma}') = \left(\frac{\partial f}{\partial \bar{\sigma}'}\right)^{\mathrm{T}} \mathbf{T}\mathbf{T}^{-1}\bar{\sigma}' = \left(\frac{\partial f}{\partial \bar{\sigma}'}\right)^{\mathrm{T}} \bar{\sigma}' = 2f' = 2f. \tag{13}$$

Thus, employing (13) and (5) in (9), we have

$$\dot{\varepsilon}^{\mathrm{p}}_{\mathrm{eq}} = \frac{\dot{\lambda}}{\sigma_{\mathrm{eq}}}(2f) = \frac{\dot{\lambda}}{\sigma_{\mathrm{eq}}} \cdot 2 \cdot \tfrac{2}{3}\sigma^2_{\mathrm{eq}} = \tfrac{4}{3}\dot{\lambda}\sigma_{\mathrm{eq}}. \tag{14}$$

For the present case of time-independent small-deformation elasto-plasticity, the total strain increment can be linearly decomposed into elastic and plastic strain increments. That is,

$$\dot{\varepsilon}_j = \dot{\varepsilon}^{\mathrm{e}}_j + \dot{\varepsilon}^{\mathrm{p}}_j \quad (j = 1, 2, 6). \tag{15}$$

Now, because of the reversible nature of the elastic strain increment

$$\dot{\sigma}_i = c_{ij}\dot{\varepsilon}^{\mathrm{e}}_j = c_{ij}(\dot{\varepsilon}_j - \dot{\varepsilon}^{\mathrm{p}}_j) = c_{ij}\dot{\varepsilon}_j - c_{ij}\dot{\lambda}\frac{\partial f}{\partial \sigma_j} \quad (i, j = 1, 2, 6), \tag{16}$$

where relation (15) above and the associated flow rule have been used.

Substituting the last two results in (4), we get

$$\frac{\partial f}{\partial \sigma_i} c_{ij}\dot{\varepsilon}_j - \frac{\partial f}{\partial \sigma_i} c_{ij} \frac{\partial f}{\partial \sigma_j}\dot{\lambda} - \frac{\partial k}{\partial \varepsilon^{\mathrm{p}}_{\mathrm{eq}}} \frac{4}{3}\dot{\lambda}\sigma_{\mathrm{eq}} = 0, \tag{17}$$

whence

$$\dot{\lambda} = \frac{\dfrac{\partial f}{\partial \sigma_i} c_{ij}\dot{\varepsilon}_j}{\dfrac{\partial f}{\partial \sigma_i} c_{ij} \dfrac{\partial f}{\partial \sigma_j} + \dfrac{\partial k}{\partial \varepsilon^{\mathrm{p}}_{\mathrm{eq}}} \dfrac{4}{3}\sigma_{\mathrm{eq}}}. \tag{18}$$

Substituting the above in (16) we arrive at our final form of the elasto-plastic constitutive relation:

$$\dot{\sigma}_i = \left[c_{ij} - \frac{c_{ik} \dfrac{\partial f}{\partial \sigma_k} \dfrac{\partial f}{\partial \sigma_m} c_{mj}}{\dfrac{\partial f}{\partial \sigma_k} c_{km} \dfrac{\partial f}{\partial \sigma_m} + \dfrac{\partial k}{\partial \varepsilon^{\mathrm{p}}_{\mathrm{eq}}} \dfrac{4}{3}\sigma_{\mathrm{eq}}} \right] \dot{\varepsilon}_j. \tag{19}$$

It should be noted that strain-hardening is incorporated in the elasto-plastic model given by the above equation through the term $\partial k/\partial \varepsilon^{\mathrm{p}}_{\mathrm{eq}}$. Hence an explicit expression for this term is necessary. In the present case, hardening is represented by the following three-parameter model suggested by Kenaga *et al.* (1987) for a Boron–Aluminum composite:

$$k = \tfrac{2}{3}\sigma^2_{\mathrm{eq}} = \tfrac{2}{3}\{\alpha^{\beta}\varepsilon^{\mathrm{p}}_{\mathrm{eq}} + (\sigma^{\mathrm{Y}}_{\mathrm{eq}})^{\beta}\}^{2/\beta}, \tag{20}$$

where α, β and $\sigma^{\mathrm{Y}}_{\mathrm{eq}}$ are determined experimentally. The quantity σ^{Y}_{eq} is actually the equivalent stress at incipient yielding.

From the above relation one obtains

$$\frac{\partial k}{\partial \varepsilon_{eq}^{p}} = \frac{4}{3}\frac{\alpha^{\beta}}{\beta}\sigma_{eq}^{2-\beta}. \tag{21}$$

Hence the elasto-plastic constitutive relation for incremental stresses and strains can be written concisely as

$$\dot{\sigma}_i = c_{ij}^{ep}\dot{\varepsilon}_j, \tag{22}$$

where

$$c_{ij}^{ep} = c_{ij} - \frac{c_{ik}\dfrac{\partial f}{\partial \sigma_k}\dfrac{\partial f}{\partial \sigma_m}c_{mj}}{\dfrac{\partial f}{\partial \sigma_k}c_{km}\dfrac{\partial f}{\partial \sigma_m} + \dfrac{16}{9}\dfrac{\alpha^{\beta}}{\beta}\sigma_{eq}^{3-\beta}}\dot{\varepsilon}_j. \tag{22a}$$

Equation (22a) can be expressed for plane stress as well as plane strain by a suitable adjustment of the fourth component of stress and strain in the usual manner.

INITIAL STRESS BOUNDARY ELEMENT FORMULATION

The basic boundary element equation for small-deformation elasto-plastic analysis is given by Banerjee *et al.* (1979) and Banerjee and Butterfield (1981) for the initial stress approach. In the present case, elasto-plastic behavior may be caused by mechanical and thermal body force loading in addition to surface loading. Since the body force loading is accounted for by a particular integral-based formulation (Deb and Banerjee, 1990), the basic boundary element equation in terms of incremental complementary tractions and displacements becomes

$$\mathscr{C}_{ij}(\xi_0)\dot{u}_i^c(\xi_0) = \int_S [G_{ij}(x,\xi_0)\dot{t}_i^c(x) - F_{ij}(x,\xi_0)\dot{u}_i^c(x)]\,dS(x) + \int_V B_{ikj}(x,\xi_0)\dot{\sigma}_{ik}^0(x)\,dV(x),$$
$$(i,j,k = 1,2). \tag{23}$$

The necessary interior stress equation is

$$\dot{\sigma}_{ij}(\xi) = \int_S [G_{kij}^{\sigma}(x,\xi)\dot{t}_k^c(x) - F_{kij}^{\sigma}(x,\xi)\dot{u}_k^c(x)]\,dS(x) + \int_V B_{klij}^{\sigma}(x,\xi)\dot{\sigma}_{kl}^0(x)\,dV(x),$$
$$(i,j,k = 1,2). \tag{24}$$

The kernel functions G_{ij} and F_{ij} are defined in Deb and Banerjee (1990). The remaining quantities B_{ikj}, B_{klij}^{σ}, G_{kij}^{σ} and F_{kij}^{σ} can be derived from G_{ij} by taking appropriate spatial derivatives and utilizing the stress–strain relations in a straightforward manner. Because these expressions are lengthy and could not be expressed in a condensed form, they are not reproduced here.

For our purpose it is convenient to use the contracted notation for stress followed earlier. According to this notation a pair of consecutive indices [say, (ij)] is equivalent to a single index (say, m) as follows:

$$ij \equiv ji \Rightarrow m,$$

meaning

$$11 \Rightarrow 1,$$
$$22 \Rightarrow 2,$$
$$12 \equiv 21 \Rightarrow 6.$$

With the above notation the cardinal equations, (23) and (24) above, are rewritten below:

$$\mathscr{C}_{ij}(\xi_0)\dot{u}_i^c(\xi_0) = \int_S [G_{ij}(x,\xi_0)\dot{t}_i^c(x) - F_{ij}(x,\xi_0)\dot{u}_i^c(x)]\,\mathrm{d}S(x) + \int_V \mathscr{B}_{mj}(x,\xi_0)\dot{\sigma}_m^0(x)\,\mathrm{d}V(x), \tag{25}$$

$$\dot{\sigma}_m(\xi) = \int_S [\mathscr{G}_{km}^{\sigma}(x,\xi)\dot{t}_k^c(x) - \mathscr{F}_{km}^{\sigma}(x,\xi)\dot{u}_k^c(x)]\,\mathrm{d}S(x) + \int_V \mathscr{B}_{nm}^{\sigma}(x,\xi)\dot{\sigma}_n^0(x)\,\mathrm{d}V(x),$$

$$(m,n = 1,2,6). \tag{26}$$

The initial stress rate $\dot{\sigma}_i^0$ appearing in eqns (25) and (26) above is defined as the difference between the pseudo (or elastic) and actual stress rates. That is,

$$\dot{\sigma}_i^0 = \dot{\sigma}_i^e - \dot{\sigma}_i, \tag{27}$$

where

$$\dot{\sigma}_i^e = c_{ij}\dot{\varepsilon}_j, \tag{27a}$$

and $\dot{\sigma}_i$ is given either by eqn (22) or because of the recoverable nature of the elastic strain component $\dot{\varepsilon}_i^e$ is also given as follows:

$$\dot{\sigma}_i = c_{ij}\dot{\varepsilon}_j^e. \tag{28}$$

Employing the last two relations in eqn (27) in conjunction with the linear decomposition relation [as given by (15)] for the total strain increment one gets the following:

$$\dot{\sigma}_i^0 = c_{ij}\dot{\varepsilon}_j^p. \tag{29}$$

Substituting the plastic flow rule (8) in the above equation it is possible to write the following representation of incremental initial stress:

$$\dot{\sigma}_i^0 = K_i\dot{\lambda}, \tag{30}$$

where

$$K_i = c_{ij}\frac{\partial f}{\partial \sigma_j}. \tag{30a}$$

The last two equations above along with the vector L_i to be defined below are of special interest for our final development of the variable stiffness type boundary element equations for numerical implementation. Incorporating relations (21) and (14) into the consistency condition (4), we get

$$\frac{\partial f}{\partial \sigma_i}\dot{\sigma}_i - \left(\frac{4}{3}\frac{\alpha^\beta}{\beta}\sigma_{eq}^{2-\beta}\right)\left(\tfrac{4}{3}\dot{\lambda}\sigma_{eq}\right) = 0. \tag{31}$$

From the above equation we obtain

$$\dot{\lambda} = L_i^{\sigma}\dot{\sigma}_i, \tag{32}$$

where

$$L_i^\sigma = \frac{9}{16}\frac{\beta}{\alpha^\beta}\sigma_{eq}^{\beta-3}\frac{\partial f}{\partial \sigma_i}. \tag{32a}$$

By utilizing relation (30) in eqns (25) and (26), and relation (32) in eqn (26), we get the following equations on boundary and interior respectively:

$$\mathscr{C}_{ij}(\xi_0)\dot{u}_i^c(\xi_0) = \int_S [G_{ij}(x,\xi_0)\dot{t}_i^c(x) - F_{ij}(x,\xi_0)\dot{u}_i^c(x)]\,dS(x) + \int_V \mathscr{B}_{mj}(x,\xi_0)K_m(x)\dot{\lambda}(x)\,dV(x), \tag{33}$$

$$\dot{\lambda}(\xi) = L_m^\sigma(\xi)\int_S [\mathscr{G}_{km}^\sigma(x,\xi)\dot{t}_k^c(x) - \mathscr{F}_{km}^\sigma(x,\xi)\dot{u}_k^c(x)]\,dS(x) + L_m^\sigma(\xi)\int_V \mathscr{B}_{nm}^\sigma(x,\xi)K_n(x)\dot{\lambda}(x)\,dV(x), \quad (m,n = 1,2,6). \tag{34}$$

The isotropic counterparts of eqns (33) and (34) are given in Banerjee and Raveendra (1987) for plane problems, by Henry and Banerjee (1988) for axisymmetric problems and by Banerjee *et al.* (1989) for three-dimensional problems.

NUMERICAL IMPLEMENTATION

The integral equations presented in the foregoing become amenable to solution only after proper numerical implementation is carried out. Typically, in a nonlinear boundary element solution procedure, the nonlinear region of the problem domain is physically divided into "cells" and the bounding surface into "boundary elements". In a substructured analysis, the domain of the problem may be divided into two or more subregions and boundary element equations such as (33) and (34) are written for each subregion. The final system results from enforcing displacement and traction compatibilities along the interfaces between subregions (Banerjee and Butterfield, 1981). In the present boundary and volume discretization of the relevant integrals, quadratic isoparametric shape functions are used to approximate the geometry and the field variables across the boundary elements and over volume cells in terms of their nodal values. Thus after discretization, eqn (33) can be expressed in the following manner:

$$\mathscr{C}_{ij}(\xi_0)\dot{u}_i^c(\xi_0) = \sum_{q=1}^{NB}\left[\int_{S(q)} [G_{ij}(x,\xi_0)N^\gamma(\eta^S)\,dS^{(q)}](\dot{\bar{t}}_i^c)^{\gamma(q)}\right] - \sum_{q=1}^{NB}\left[\int_{S(q)} [F_{ij}(x,\xi_0)N^\gamma(\eta^S)\,dS^{(q)}](\dot{\bar{u}}_i^c)^{\gamma(q)}\right] + \sum_{p=1}^{NV}\left[\int_{V(p)} \mathscr{B}_{mj}(x,\xi_0)N^\beta(\eta^V)\,dV^{(p)}\right]K_m\dot{\lambda}^{\beta(p)}, \tag{35}$$

where, NB = number of boundary elements, NV = number of volume cells, $N^\gamma(\eta^S)$ represents boundary element shape functions of quadratic variation and $N^\beta(\eta^V)$ represents quadratic shape functions for cells (of same dimensions as those of the analysis). The bars indicate nodal values and the integration coordinate x has been expressed in local coordinates η^S or η^V via the above shape functions. It should be noted that non-repeating indices in equation (35) are enclosed in parentheses. The indices γ and β extend over the total number of nodes in a boundary element and a volume cell respectively. After carrying out the necessary numerical integration by advanced self-adaptive Gaussian quadrature schemes and the indirect singular coefficient computations (Banerjee and Raveendra, 1987; Banerjee *et al.*, 1989), eqn (35) can be written in the following matrix notation:

$$\mathbf{G}\dot{\bar{t}}^c - \mathbf{F}\dot{\bar{u}}^c + \mathbf{B}\mathbf{K}\dot{\lambda} = 0. \tag{36}$$

On applying the known boundary traction and displacement increments and the particular integrals $\dot{\bar{t}}^p (= \dot{\bar{t}} - \dot{\bar{t}}^c)$ and $\dot{\bar{u}}^p (= \dot{\bar{u}} - \dot{\bar{u}}^c)$ due to mechanical as well as thermo-mechanical body forces (Deb and Banerjee, 1990; Deb *et al.*, 1991), eqn (36) above can be reduced to the following form:

$$\mathbf{A}\dot{X} + \mathbf{B}\mathbf{K}\dot{\lambda} + (\dot{b} - \mathbf{G}\dot{\bar{t}}^p + \mathbf{F}\dot{\bar{u}}^p) = 0. \tag{37}$$

Equation (37) reduces to the system equation for elastic analysis (Deb *et al.*, 1991) in the absence of any plastic deformation (i.e. $\dot{\lambda} = 0$)

$$\mathbf{A}\dot{x} = \dot{b} - \mathbf{G}\dot{\bar{t}}^p + \mathbf{F}\dot{\bar{u}}^p. \tag{38}$$

In (37) above, $\mathbf{A}$ is the assembled system matrix, $\dot{X}$ is the incremental vector of unknown displacements and tractions and $\dot{b}$ is the vector derived from incremental known tractions and displacements.

The integral equation (34) which is valid for interior points can be written in a form similar to eqn (37). It is noted that since ξ in eqn (34) is a point interior to the domain the integrals involving the kernels $\mathscr{G}^{\sigma}_{km}$ and $\mathscr{F}^{\sigma}_{km}$ are nonsingular. However, strong singularity will arise in the term $\mathscr{B}^{\sigma}_{nm}$ when the volume cell includes the node at which eqn (34) is applied. Similar to the surface integral containing the F_{ij} kernel in eqn (33), the volume integral containing the $\mathscr{B}^{\sigma}_{nm}$ kernel in eqn (34) exists in the Cauchy principal value sense together with an analytic jump term. Utilizing a technique similar to that used for indirect computation of the singular coefficients related to the F_{ij} kernel (Rizzo and Shippy, 1968; Watson, 1979; Banerjee and Butterfield, 1981), the singular terms corresponding to the $\mathscr{B}^{\sigma}_{nm}$ kernel can be computed. This approach was initially used for these types of kernels by Henry and Banerjee (1988) and Banerjee *et al.* (1989) who named it as the "initial stress expansion technique". The initial stresses chosen are such that the resultant real stresses are zero while a non-zero displacement field exists similar to the situation in which a body is allowed to undergo free thermal expansion under the application of a uniform temperature distribution. The initial stress states that can be used in the present case are described in Table 1. On carrying out the necessary numerical integrations, eqn (34) can be written in matrix form for all interior nodes as:

$$\dot{\lambda} = \mathbf{L}^{\sigma}(\mathbf{G}^{\sigma}\dot{\bar{t}}^c - \mathbf{F}^{\sigma}\dot{\bar{u}}^c + \mathbf{B}^{\sigma}\mathbf{K}\dot{\lambda}). \tag{39}$$

On incorporating the known boundary traction and displacement increments and the relevant particular integrals due to mechanical body forces, if any, the above equation may be transformed to the following form:

$$\mathbf{L}^{\sigma}\mathbf{A}^{\sigma}\dot{X} + (\mathbf{L}^{\sigma}\mathbf{B}^{\sigma}\mathbf{K} - \mathbf{I})\dot{\lambda} + \mathbf{L}^{\sigma}(\dot{b}^{\sigma} - \mathbf{G}^{\sigma}\dot{\bar{t}}^p + \mathbf{F}^{\sigma}\dot{\bar{u}}^p) = 0, \tag{40}$$

where

$$\mathbf{G}^{\sigma}\dot{\bar{t}} - \mathbf{F}^{\sigma}\dot{\bar{u}} = \mathbf{A}^{\sigma}\dot{X} + \dot{b}^{\sigma}. \tag{40a}$$

It is important to note here that eqn (40) as derived from eqn (34) is valid for interior cell

Table 1. Stress states for initial stress expansion technique

Stress state	Element to be determined corresponds to	Nodal values of assumed stress state				
		σ°_{11}	σ°_{22}	σ°_{12}	u_1	u_2
1	σ°_{11}	1	0	0	$b_{11}x_1 + \frac{1}{2}b_{16}x_2$	$b_{12}x_2 + \frac{1}{2}b_{16}x_1$
2	σ°_{22}	0	1	0	$b_{12}x_1 + \frac{1}{2}b_{26}x_2$	$b_{22}x_2 + \frac{1}{2}b_{26}x_1$
3	σ°_{12}	0	0	1	$b_{16}x_1 + \frac{1}{2}b_{66}x_2$	$b_{26}x_2 + \frac{1}{2}b_{66}x_1$

nodes only. This is so because for points on the boundary the kernel $\mathscr{F}^{\sigma}_{km}$ is hypersingular [of $O(1/r^2)$] and the integral involving it does not exist in the Cauchy principal value sense. Stresses on the boundary are calculated using an alternative matrix equation which can be case in the same form as eqn (40). The matrix equation for boundary stresses can be obtained with the help of a stress–strain constitutive relation, strain-displacement correspondence, stress-traction equilibrium equations and parametric derivatives of boundary displacement components as outlined below.

Writing eqn (27) for the two-dimensional case in expanded form after incorporating linear strain-displacement relations, we have the following:

$$\dot{\sigma}_1 - c_{11}\dot{u}_{1,1} - c_{12}\dot{u}_{2,2} - c_{16}\dot{u}_{1,2} - c_{16}\dot{u}_{2,1} = -\dot{\sigma}^0_1, \tag{41}$$

$$\dot{\sigma}_2 - c_{12}\dot{u}_{1,1} - c_{22}\dot{u}_{2,2} - c_{26}\dot{u}_{1,2} + c_{26}\dot{u}_{2,1} = -\dot{\sigma}^0_2, \tag{42}$$

$$\dot{\sigma}_6 - c_{16}\dot{u}_{1,1} - c_{26}\dot{u}_{2,2} - c_{66}\dot{u}_{1,2} - c_{66}\dot{u}_{2,1} = -\dot{\sigma}^0_6. \tag{43}$$

The stress-traction equilibrium relations can be written for a point lying on a particular boundary element as:

$$\dot{\sigma}_1 n_1 + \dot{\sigma}_6 n_2 = \dot{t}_1 = N^{\gamma}\dot{t}^{\gamma}_1 \quad (\gamma = 1,2,3), \tag{44}$$

$$\dot{\sigma}_6 n_1 + \dot{\sigma}_1 n_2 = \dot{t}_2 = N^{\gamma}\dot{t}^{\gamma}_2 \quad (\gamma = 1,2,3), \tag{45}$$

where N^{γ} and t^{γ}_i are respectively the γth shape function and nodal traction in the ith direction. If the shape function N^{γ} is a function of the parameter η defining the iso-parameteric boundary element under consideration, we get the following relations for derivatives of u_i with respect to η:

$$J_1\dot{u}_{1,1} + J_2\dot{u}_{1,2} = \frac{\mathrm{d}u_1}{\mathrm{d}\eta} = \frac{\mathrm{d}N^{\gamma}}{\mathrm{d}\eta}\dot{u}^{\gamma}_1 \quad (\gamma = 1,2,3), \tag{46}$$

$$J_1\dot{u}_{2,1} + J_2\dot{u}_{2,2} = \frac{\mathrm{d}u_2}{\mathrm{d}\eta} = \frac{\mathrm{d}N^{\gamma}}{\mathrm{d}\eta}\dot{u}^{\gamma}_2 \quad (\gamma = 1,2,3), \tag{47}$$

where the Jacobian of transformation between the local parameteric coordinate η and the global coordinates x_i is defined as follows:

$$J_i = x^{\gamma}_i \frac{\mathrm{d}N^{\gamma}}{\mathrm{d}\eta} \quad (i = 1,2; \quad \gamma = 1,2,3). \tag{48}$$

Let the following matrices be defined:

$$\mathbf{A}_{11} = \mathbf{I}_{3\times 3}, \tag{49}$$

$$\mathbf{A}_{12} = -\begin{bmatrix} c_{11} & c_{12} & c_{16} & c_{16} \\ c_{12} & c_{22} & c_{26} & c_{26} \\ c_{16} & c_{26} & c_{66} & c_{66} \end{bmatrix}, \tag{50}$$

$$\mathbf{A}_{21} = \begin{bmatrix} n_1 & 0 & n_2 \\ 0 & n_2 & n_1 \\ 0 & 0 & 0 \\ 0 & 0 & 0 \end{bmatrix}, \tag{51}$$

$$\mathbf{A}_{22} = \begin{bmatrix} 0 & 0 & 0 & 0 \\ 0 & 0 & 0 & 0 \\ J_1 & 0 & J_2 & 0 \\ 0 & J_2 & 0 & J_1 \end{bmatrix}. \tag{52}$$

Then it can be shown that

$$\dot{\bar{\sigma}} = -(\mathbf{A}_{11}-\mathbf{A}_{12}\mathbf{A}_{22}^{-1}\mathbf{A}_{21})^{-1}[\mathbf{A}_{12}\mathbf{A}_{22}^{-1}\dot{\bar{\mathbf{r}}}+\dot{\bar{\sigma}}^0], \tag{53}$$

where

$$\dot{\bar{\sigma}}^0 = \{\dot{\sigma}_1^0 \quad \dot{\sigma}_2^0 \quad \dot{\sigma}_6^0\}^{\mathrm{T}}, \tag{53a}$$

$$\dot{\bar{\mathbf{r}}} = \left\{N^\gamma \dot{t}_1^\gamma \quad N^\gamma \dot{t}_2^\gamma \quad \frac{\mathrm{d}N^\gamma}{\mathrm{d}\eta}\ddot{u}_1^\gamma \quad \frac{\mathrm{d}N^\gamma}{\mathrm{d}\eta}\ddot{u}_2^\gamma\right\}. \tag{53b}$$

While eqn (26) is strictly applicable to an interior point, eqn (53) above is to be employed for calculating stresses on a boundary point for the two-dimensional case. Equation (53) can subsequently be transformed to the same form as eqn (40) on incorporating relations (30) and (32). Hence, the final equation of the form (40) is assumed to include all the interior and boundary cell nodes of the discretized problem domain.

NEWTON–RAPHSON ITERATIVE SOLUTION

Equations (37) and (40) are of primary interest for obtaining a solution to the elasto-plastic stress analysis problem by a procedure which will now be described. This procedure closely follows the methodology developed by Chopra (1991), and Chopra and Dargush (1992). Before going into the details of the numerical algorithm, it is convenient to write the pertinent equations in a somewhat more compact form for easy reference as given below:

$$\mathbf{A}\dot{\bar{X}}+\mathbf{B}\mathbf{K}\dot{\bar{\lambda}}+\dot{\bar{p}} = 0, \tag{54}$$

$$\mathbf{L}^\sigma\mathbf{A}^\sigma\dot{\bar{X}}+(\mathbf{L}^\sigma\mathbf{B}^\sigma\mathbf{K}-\mathbf{I})\dot{\bar{\lambda}}+\mathbf{L}^\sigma\dot{\bar{p}}^\sigma = 0, \tag{55}$$

where

$$\dot{\bar{p}} = \dot{\bar{b}}-\mathbf{G}\dot{\bar{t}}^{\mathrm{p}}+\mathbf{F}\dot{\bar{u}}^{\mathrm{p}}, \tag{54a}$$

$$\dot{\bar{p}}^\sigma = \dot{\bar{b}}^\sigma-\mathbf{G}^\sigma\dot{\bar{t}}^{\mathrm{p}}+\mathbf{F}^\sigma\dot{\bar{u}}^{\mathrm{p}}. \tag{55a}$$

It is to be noted that $\dot{\bar{X}}$ and $\dot{\bar{\lambda}}$ cannot be determined by solving eqns (54) and (55) in one step as $\mathbf{L}^\sigma$ and $\mathbf{K}$ which are parts of the coefficient matrices are functions of the current stresses which are themselves unknown. Equations (54) and (55) despite their incremental form are thus nonlinear. An iterative algorithm of the Newton–Raphson type can be used to arrive at the correct solution for these equations. The aim of the current approach as is true for most iterative analyses is to begin with approximate values of the unknowns and successfully improve them to obtain converged results within a preassigned tolerance. Thus, for any mth iteration the following residues or error-terms are defined:

$$\bar{R}(\dot{\bar{X}}^m, \dot{\bar{\lambda}}^m) = \mathbf{A}\dot{\bar{X}}^m+\mathbf{B}\mathbf{K}\dot{\bar{\lambda}}^m+\dot{\bar{p}} \neq 0, \tag{56}$$

$$\bar{R}^\sigma(\dot{\bar{X}}^m, \dot{\bar{\lambda}}^m) = \mathbf{L}^\sigma\mathbf{A}^\sigma\dot{\bar{X}}^m+(\mathbf{L}^\sigma\mathbf{B}^\sigma\mathbf{K}-\mathbf{I})\dot{\bar{\lambda}}^m+\mathbf{L}^\sigma\dot{\bar{p}}^\sigma \neq 0. \tag{57}$$

Linearized Taylor's series expansions are next assumed about the residues for the mth iteration and these are set to zero to meet the goal of satisfying the equalities (54) and (55). Thus we have, neglecting the higher order terms in the expansions referenced above,

$$\bar{R}(\dot{\bar{X}}, \dot{\lambda}) = \bar{R}(\dot{\bar{X}}^m, \dot{\lambda}^m) + \frac{\partial \bar{R}}{\partial \dot{\bar{X}}}(\Delta \dot{\bar{X}}^m) + \frac{\partial \bar{R}}{\partial \dot{\lambda}}(\Delta \dot{\lambda}^m) = 0, \tag{58}$$

$$\bar{R}^\sigma(\dot{\bar{X}}, \dot{\lambda}) = \bar{R}^\sigma(\dot{\bar{X}}^m, \dot{\lambda}^m) + \frac{\partial \bar{R}}{\partial \dot{\bar{X}}}(\Delta \dot{\bar{X}}^m) + \frac{\partial \bar{R}^\sigma}{\partial \dot{\lambda}}(\Delta \dot{\lambda}^m) = 0. \tag{59}$$

The above two equations can be grouped together as

$$\begin{bmatrix} \mathbf{A} & \mathbf{BK} \\ \mathbf{L}^\sigma \mathbf{A}^\sigma & \mathbf{L}^\sigma \mathbf{B}^\sigma \mathbf{K} - \mathbf{I} \end{bmatrix} \begin{Bmatrix} \Delta \dot{\bar{X}}^m \\ \Delta \dot{\lambda}^m \end{Bmatrix} = - \begin{Bmatrix} \bar{R}(\dot{\bar{X}}^m, \dot{\lambda}^m) \\ \bar{R}^\sigma(\dot{\bar{X}}^m, \dot{\lambda}^m) \end{Bmatrix}. \tag{60}$$

The iterative solution procedure can now be described by the following steps (I) through (IV):

(I) Obtain **G**, $\mathbf{G}^\sigma$, **F**, $\mathbf{F}^\sigma$, **A**, $\mathbf{A}^\sigma$, **B** and $\mathbf{B}^\sigma$ for the given problem.

(II) Apply an increment of surface and body force loadings and calculate $\dot{p}$ and $\dot{p}^\sigma$. Solve for $\dot{\bar{X}}$ from eqn (54) with $\dot{\lambda} = 0$. Compute interior stress increments using the alternative form of eqn (55) which can be deduced directly from eqn (26). In this case, $\dot{\lambda} = 0$ needs to be substituted in the following equation:

$$\dot{\sigma}^e = \mathbf{A}^\sigma \dot{\bar{X}} + \mathbf{B}^\sigma \mathbf{K} \dot{\lambda} + \dot{p}^\sigma, \tag{61}$$

where the superscript e indicates the elastic nature of the stress increment. The stresses are next updated to obtain the total elastic stresses.

(III) At this stage, a check for yielding is carried out at all nodal points after calculating the equivalent stress σ_{eq} at each point. One of the following cases (a), (b) or (c) may arise for every point under consideration:

(a) $\sigma_{eq} > \sigma_{eq}^Y$.

Find the scale factor (ESF) to determine the elastic part of the stress increment:

$$\text{ESF} = 1 - \frac{\sigma_{eq} - \sigma_{eq}^Y}{\sigma_{eq}}. \tag{62}$$

Compute the incorrect part of the stress increment, that is, $(1 - \text{ESF})\dot{\sigma}_i^e$ beyond the yield surface. This part is denoted as $\dot{\sigma}_i^e$ in the beginning of the iteration process described in step (IV).

(b) $\sigma_{eq} = \sigma_{eq}^Y$.

Yielding has just occurred. So correct stress increment has been obtained and no adjustment is necessary.

(c) $\sigma_{eq} < \sigma_{eq}^Y$.

No yielding has occurred. The point under consideration is within the yield surface and hence correct elastic stress increment has been obtained.

At the end of the present step, a list of points which have yielded is compiled. The control is then transferred to step (IV) below. If one or more points have just yielded and the remaining are elastic, the next load increment is applied and steps (II) and (III) are repeated. The same also applies if all cell nodes are elastic.

(IV) During the mth iteration, for points which have yielded, elastic strain increment is determined as follows:

$$(\dot{\varepsilon}_i)^m = b_{ij}(\dot{\sigma}_i^e)^m. \tag{63}$$

The actual stress increment along the elasto-plastic path is then determined from the

following relation by using a Kutta–Simpson integration rule (Chopra, 1991; Chopra and Dargush, 1992):

$$(\dot{\sigma}_i)^m = \int_0^{(\dot{\varepsilon}_j)^m} c_{ij}^{ep}(\sigma_i)\, \mathrm{d}(\dot{\varepsilon}_j)^m. \tag{64}$$

The initial stress increment is then given as

$$(\dot{\sigma}_i^0)^m = (\dot{\sigma}_i^e)^m - (\dot{\sigma}_i)^m. \tag{65}$$

Current total stresses are obtained by adding the stress increments (64) to the previous correct total stresses and $\mathbf{L}^\sigma$ and $\mathbf{K}$ are computed. Equation (60) is now solved yielding $\Delta\dot{X}^m$ and $\Delta\dot{\lambda}^m$. These are next added as corrections to the existing vectors, $\dot{X}^m$ and $\dot{\lambda}^m$. Thus,

$$\dot{X} = \dot{X}^m + \Delta\dot{X}^m, \tag{66}$$

$$\dot{\lambda} = \dot{\lambda}^m + \Delta\dot{\lambda}^m. \tag{67}$$

The new initial stress increment is computed using relation (30) at every plastic nodal point. (Note that initial stresses are zero for points that have not yielded). The elastic stress increment is computed from eqn (61) by using $\dot{X}$ and $\dot{\lambda}$ obtained above. The steps indicated by eqns (63), (64) and (65) at the beginning of (IV) are repeated and the initial stress increment obtained from eqn (65) is compared with the previous initial stress increment to determine convergence. If convergence has not been achieved, the procedure onwards of eqn (65) is continued. Otherwise the next load step is applied, $\dot{X}$ and $\dot{\lambda}$ are calculated using eqns (54) and (55) as part of the acceleration process after having computed $\mathbf{L}^\sigma$ and $\mathbf{K}$ on the basis of the previous converged stresses, and step (IV) is restarted.

NUMERICAL EXAMPLES

Uniaxial plane stress loading of Boron–Aluminum composite

The boundary element model is a simple square plate with one quadratic cell with one quadratic three-noded boundary element per side. The side along the x_2-axis is restrained from movement in the x_1-direction while uniform traction in the x-direction is applied on the opposite side (Fig. 1). To restrain rigid body movements in the x_2-direction a roller support is applied in the x_2-direction at the midpoint of the side with applied tractions. The material properties were given by Kenaga *et al.* (1987) for the generalized Hill's criterion with isotropic hardening as:

$$E_1 = 29.4 \text{ msi}, \quad E_2 = 19.1 \text{ msi} = E_3,$$

$$\nu_{23} = \nu_{13} = \nu_{12} = 0.17, \quad G_{23} = G_{13} = G_{12} = 7.49 \text{ msi},$$

$$F_{11} = 0.001, \quad F_{22} = F_{33} = 1.0, \quad F_{23} = -0.5,$$

$$F_{13} - F_{12} = -0.01, \quad F_{44} = F_{55} = F_{66} = 1.9,$$

$$\sigma_{eq}^Y = 13.5 \text{ ksi}, \quad \alpha = 60.0 \text{ ksi}, \quad \beta = 5.8.$$

The results for the iterative Newton–Raphson boundary element analysis are presented

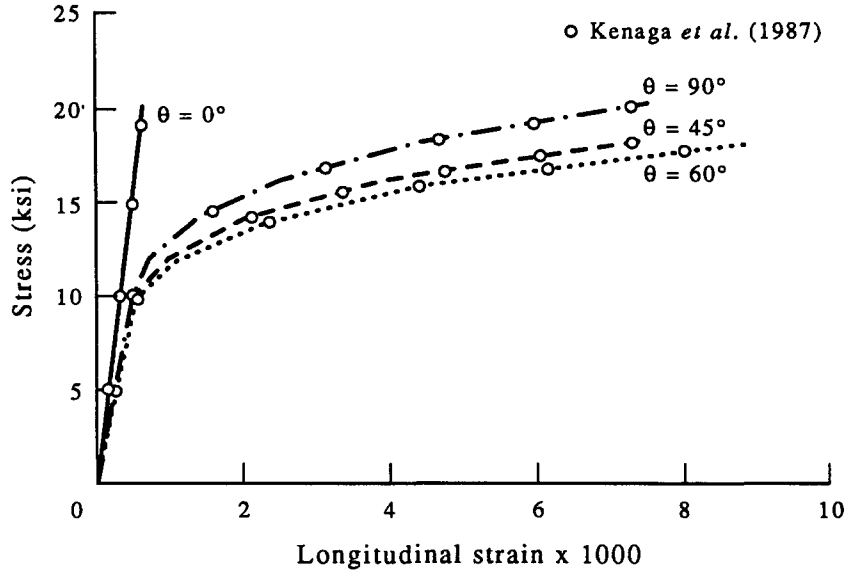

Fig. 2. Plane stress results for a uniaxial problem.

in Fig. 2 for various inclinations of the major principal axis x_1' to the loading axis x_1. Organic ultra-high strength fibers are virtually elastic up to failure and hence under uniaxial loading in the fiber direction, the composite stress-strain curve is linear up to an inordinately high value of uniaxial stress (not shown here) and only marginally nonlinear henceforth. It has been observed (Kenaga *et al.*, 1987) on the other hand that the onset of yielding is early for the off-axis loading conditions. It is of interest to observe from Fig. 2 that the composite material is actually stiffer under elasto-plastic conditions for the spatially orthotropic case of $\theta = 90°$ than for the cases of $\theta = 45°$ and 60°. It can also be seen in Fig. 2 that the results of the plane stress boundary element analysis are in very good agreement with the analytical results of Kenaga *et al.* (1987) obtained after fitting experimental data. A further confirmation of the uniaxial stress at which yielding is initiated is obtained from the loci of yield surfaces (in the first quadrant) presented in Fig. 3 for incipient yielding.

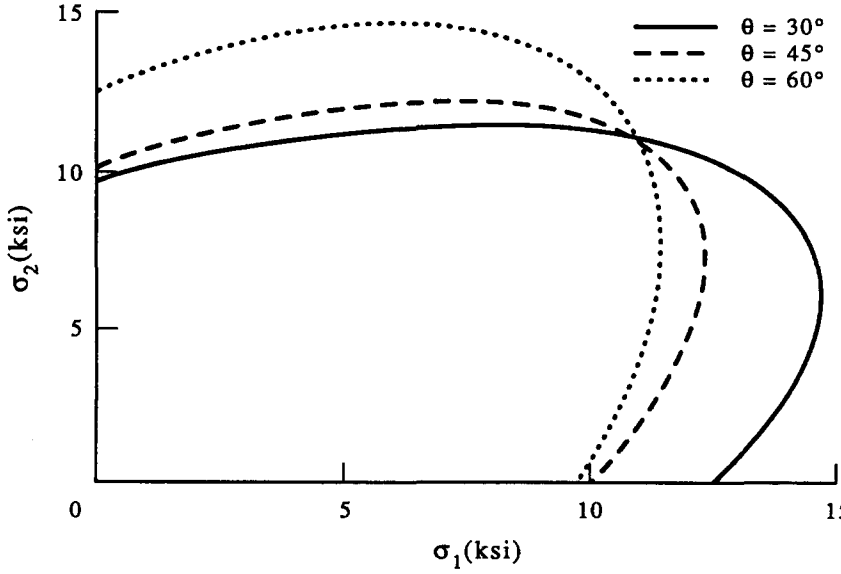

Fig. 3. Traces of yield surface for off-axis directions.

Under a biaxial plane stress condition, the equation of the yield surface for the initial state of yielding is as follows for the material under consideration:

$$\sigma_2 = \pm 13.5\sqrt{\frac{2}{3Q}}, \tag{68}$$

where

$$Q = 0.001(X\cos^2\theta + \sin^2\theta)^2 + (X\sin^2\theta + \cos^2\theta)^2 + 3.8(-X\sin\theta\cos\theta + \sin\theta\cos\theta)^2, \tag{69}$$

$$X = \frac{\sigma_1}{\sigma_2}. \tag{70}$$

The yield surfaces shown in Fig. 3 are essentially sections of ellipse represented by eqn (69). The intersection of a yield surface with the σ_1-axis represents the yield stress for the corresponding uniaxial loading configuration.

Cantilever under uniformly distributed loading (UDL) and self-weight

The example chosen here illustrates the applicability of the elasto-plastic boundary element formulation for inertial body force loading accounted for by particular integrals. The geometry of the fixed-ended cantilever chosen for the present study is shown in Fig. 4. The cantilever of mass density "ρ" is analysed under two loading conditions: (a) inertial body force loading due to self-weight (by gradually applying the acceleration due to "g" in steps) and (b) equivalent UDL ($= -10\rho g$) in the form of uniform traction on one of the longitudinal sides. A typical boundary element mesh is given in Fig. 5 where there are 20 quadratic boundary elements and 16 volume cells. (It should be noted that the boundary conditions not shown imply zero tractions.) The elasto-plastic behavior of the cantilever is represented in Fig. 6 assuming the properties of the Boron–Aluminum composite given in the example above. It is seen that the results of the inertial body force analysis are in complete agreement with the surface loading analysis due to the uniformly applied traction on the side of the beam shown in Fig. 5, thus validating the correctness of the developed analysis.

A perforated plate in tension

An example of a perforated plate will now be presented to demonstrate the consistency of the Newton–Raphson boundary element formulation presented in the foregoing. For the case of minimal anisotropy such as a small perturbation of isotropic properties, the anisotropic elasto-plastic BEM can be used after suitably reducing the quadratic stress model to the von Mises' criterion as mentioned earlier. The present Newton–Raphson BEM for this perturbed anisotropy is compared with the well-tested first generation secant type of iterative BEM (Banerjee and Butterfield, 1981) employing von Mises' yield criterion in

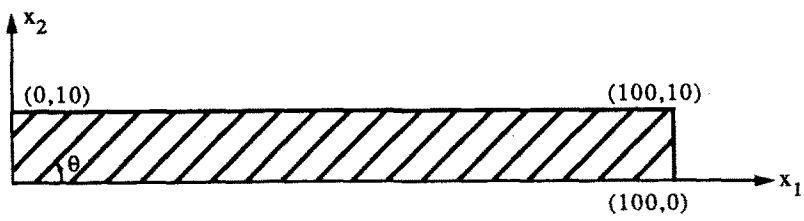

Fig. 4. Orientation of fibers in a cantilever.

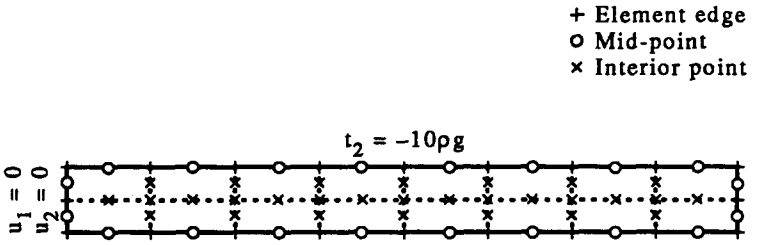

Fig. 5. Boundary element model for elastoplastic analysis.

conjunction with isotropic hardening. This comparison of two different numerical procedures serves to check the general correctness of the current numerical implementation. For the same geometric configuration results are then presented for true orthotropy.

A rectangular plate of dimensions 56×20 in. with a hole of radius $a = 5$ in. at the center subject to tension in the longer direction due to applied tractions on the smaller sides is considered. Due to symmetry under isotropic or spatially orthotropic conditions, only a quarter of the plate needs to be analysed. The plate is assigned the following material properties:

Isotropic with von Mises' criterion and hardening modulus h:

$$E = 7000 \text{ ksi}, \quad \nu = 0.2,$$
$$\sigma_y = 24.3 \text{ ksi}, \quad h = 224 \text{ ksi}.$$

Equivalent, marginally anisotropic with quadratic stress criterion:

$$E_1 = 7000.0007 \text{ ksi}, \quad E_2 = 7000 \text{ ksi}, \quad \nu_{12} = 0.2, \quad G_{12} = 2916.6666 \text{ ksi},$$
$$\sigma_{eq}^{Y} = 24.3 \text{ ksi}, \quad \alpha = 224 \text{ ksi}, \quad \beta = 1.$$

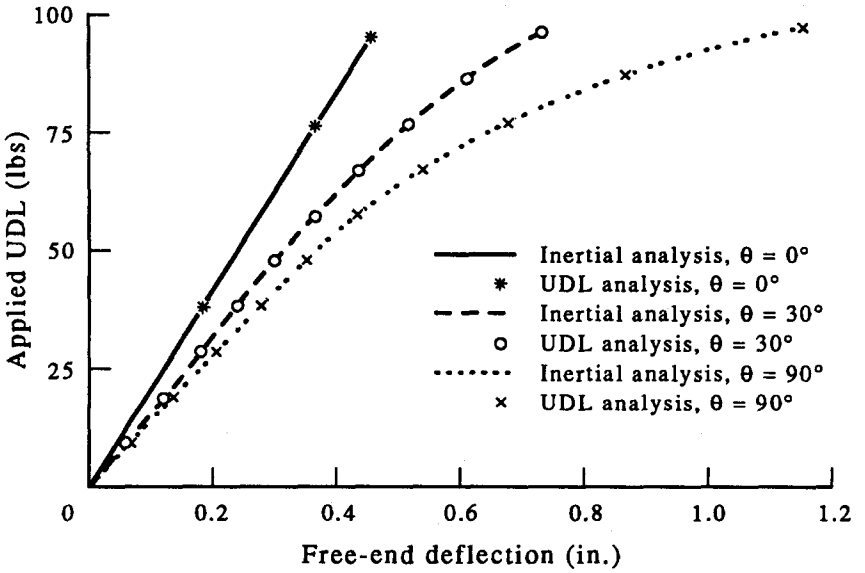

Fig. 6. Comparison between nonlinear inertial and surface loading analyses.

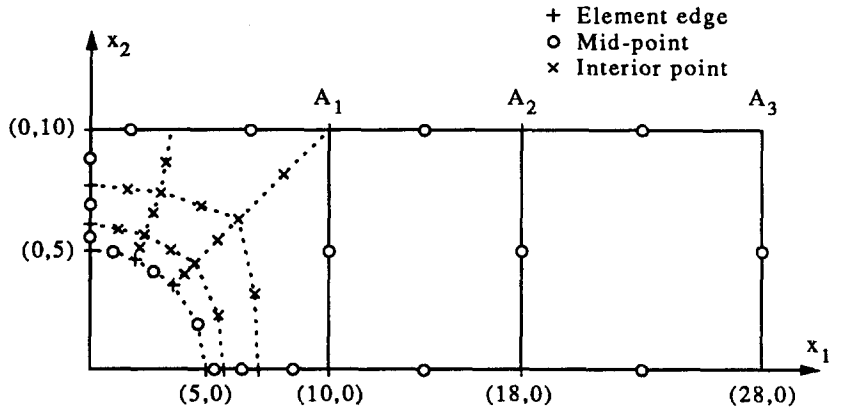

Fig. 7. Quarter plate model of a perforated plate.

The boundary element model of the quarter plate consisting of three Generic Modeling Regions (GMRs) is shown in Fig. 7. Only one of the GMRs containing the point of maximum stress, that is (0, 5), is discretized with volume cells. The remaining GMRs viz. $(10, 0)-(18, 0)-A_2-A_1$ and $(18, 0)-(28, 0)-A_3-A_2$ are discretized with boundary elements only. Thus the first GMR closest to the origin of the axes has 12 quadratic three-node boundary elements and 9 eight-node volume cells, while each of the next two GMRs has 4 three-node boundary elements. The side of the quarter plate in Fig. 7 lying along the x_1-axis is roller supported in the x_2-direction while the side along the x_2-axis is roller supported in the x_1-direction. Uniform nodal traction T_1 is applied to the side $(28, 0)-A_3$ in the x_1-direction. Comparison between the ordinary iterative BEM for isotropic von Mises' material and the present Newton–Raphson iterative BEM for perturbed anisotropy is shown in Fig. 8 in the form of a plot between the stress concentration factor at (0, 5) and percentage elongation in the x_1-direction with respect to the non-perforated plate. The first point in the curve corresponds to the elastic stress concentration factor of about 4.5. The elastic stress concentration factor is completely independent of the magnitude of the applied

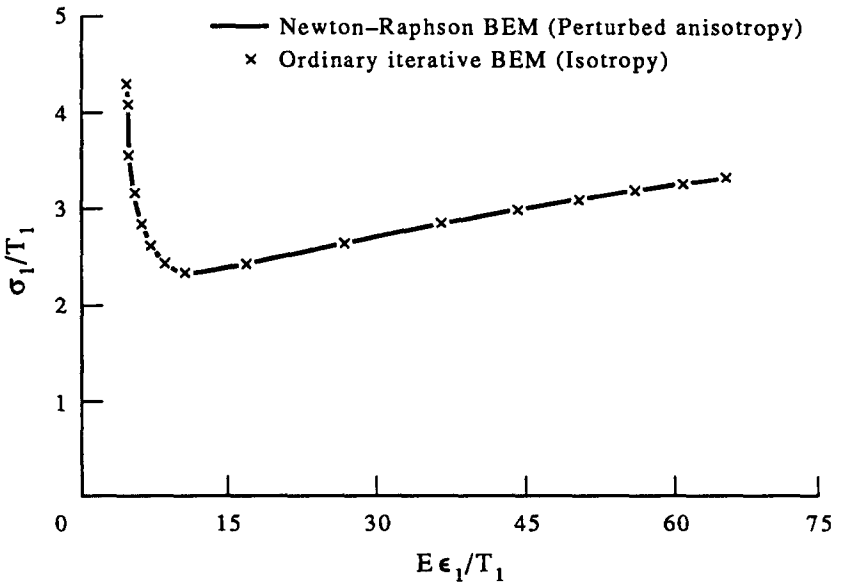

Fig. 8. Comparison of results for BEM algorithms for isotropic plate.

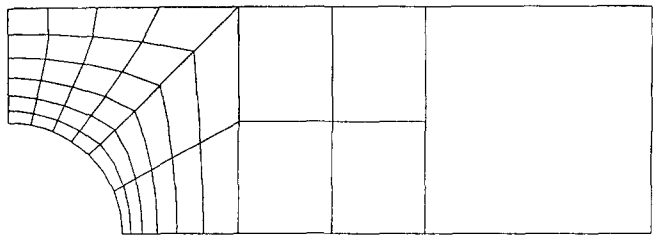

Fig. 9. Refined boundary element model of the perforated plate.

loading and is hence a single dot, that is the first tip of the curve in Fig. 8. As the plate begins to yield with gradual increase of the applied loading, the stress concentration factor falls rapidly and increases again after reaching a minimum. This variation of the stress concentration factor [σ_1/T_1 at (0, 5)] with respect to the percentage elongation ($E\varepsilon_1/T_1$ for isotropy or $E_1\varepsilon/T_1$ for perturbed anisotropy) essentially represents the effect of re-distribution of stresses due to elasto-plastic material behavior. It should be noted that since volume cells are restricted to only a part of the plate as in Fig. 7, the highest applied loading should be such that only this part of the geometry yields. The excellent agreement between the results for the ordinary iterative BEM algorithm (Banerjee and Butterfield, 1981) and the present Newton–Raphson BEM for perturbed anisotropy confirms the correctness of the latter.

The plate under consideration is analysed next for the following spatially orthotropic properties corresponding to those of a Boron–Aluminum composite (Kenaga *et al.*, 1987):

$$E_1 = 29.4 \text{ msi}, \quad E_2 = 19.1 \text{ msi}, \quad \nu_{12} = 0.17, \quad G_{12} = 7.49 \text{ msi},$$
$$F_{11} = 0.001, \quad F_{22} = 1.0, \quad F_{12} = -0.01, \quad F_{66} = 1.9,$$
$$\sigma_{eq}^{Y} = 13.5 \text{ ksi}, \quad \alpha = 60.0 \text{ ksi}, \quad \beta = 5.8.$$

In anisotropic boundary element analysis mesh size is usually a function of the inclination of fibers with respect to the loading axis. Thus a refined model with 36 and 4 cells in the first two GMRs is considered as shown in Fig. 9. It is apparent from the results (stress concentration profiles along the x_2-axis) of linear elastic analysis depicted in Figs 10 and

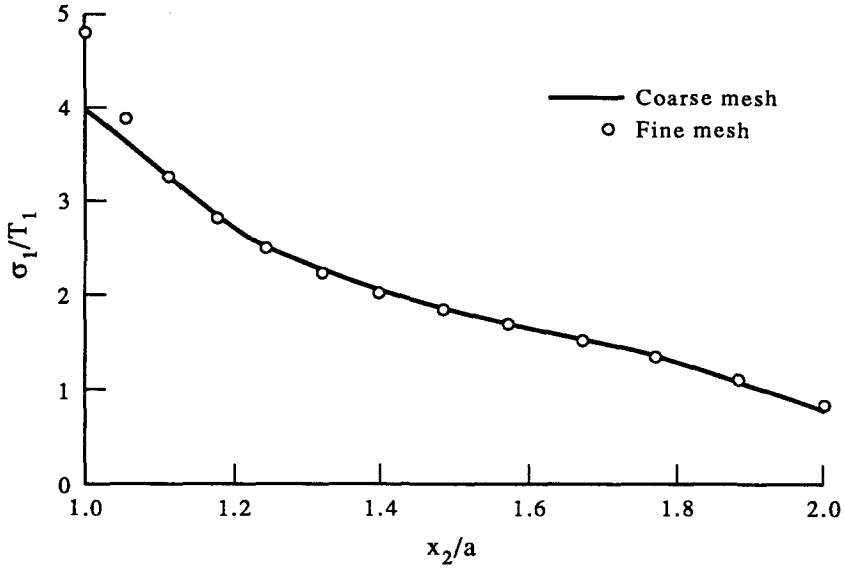

Fig. 10. Comparison of stress concentration profiles for $\theta = 0°$.

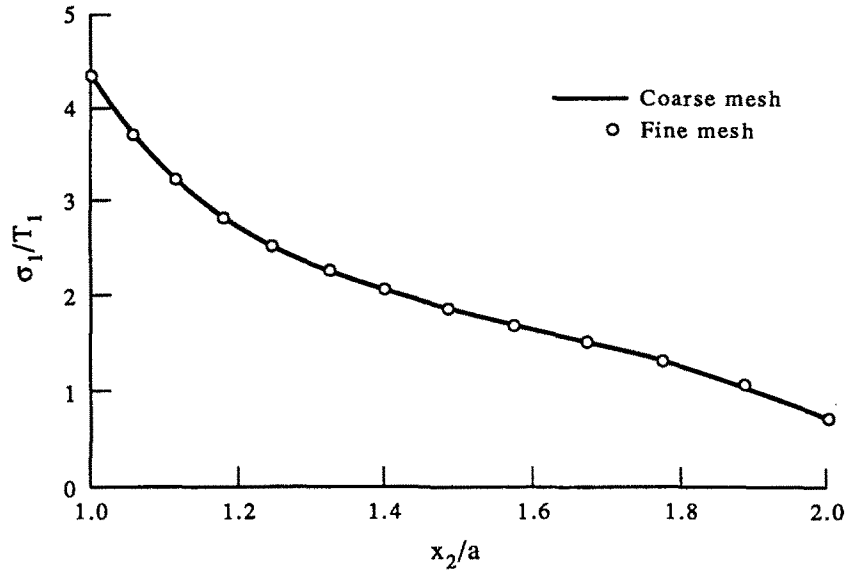

Fig. 11. Comparison of stress concentration profiles for $\theta = 90°$.

11 that convergence of stress in the proximity of the hole is not obtained for $\theta = 0°$ for the coarse mesh in Fig. 7 although the same is adequate for the $\theta = 90°$ configuration. This observation lends credence to the earlier remark that for anistropic boundary value problems, the orientation of the fibers is a controlling factor for mesh refinement. Results on elastoplastic deformation of the centrally perforated Boron–Aluminum plate are presented in Figs 12–14. These results are based on the refined boundary element model of Fig. 9. The stress–strain behavior at the root of the plate is shown in Fig. 12. The fibers being brittle and of high strength, deformation remains practically linear till fracture when loading is in the direction of fibers. The present yield criterion does not actually model the phenomenon of brittle failure. On the other hand (as can be seen in Fig. 12), the plate yields at a much lower value of stress when loaded in a direction perpendicular to the orientation

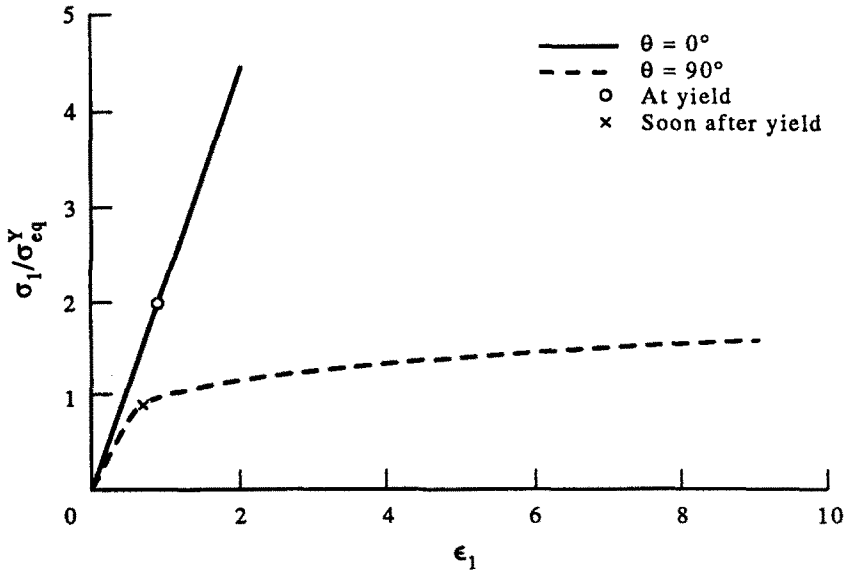

Fig. 12. Stress–strain results for the anisotropic perforated plate.

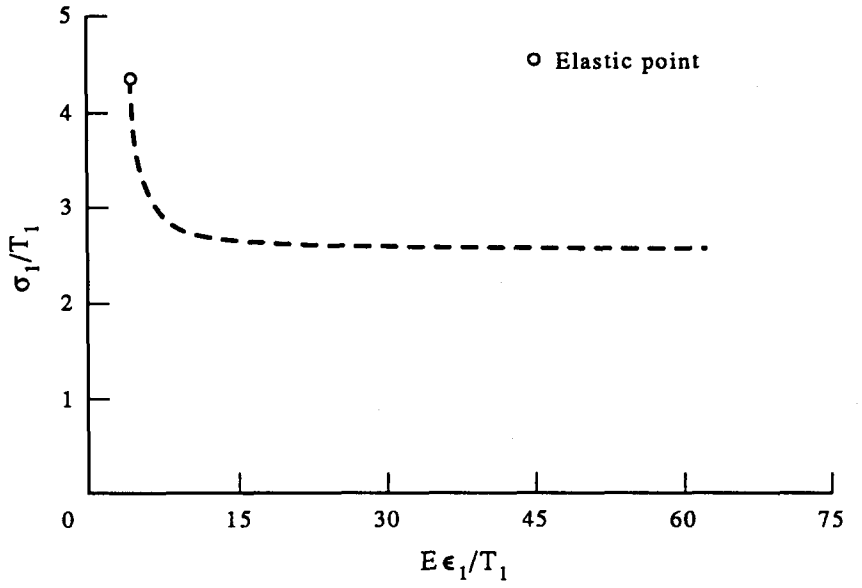

Fig. 13. Stress concentration vs strain ratio for the anisotropic plate.

of fibers ($\theta = 90°$). The variation of the plastic stress concentration factor with respect to the percentage displacement in the direction of the loading is given in Fig. 13 for $\theta = 90°$. Finally, for this same case the growing uniformity of the stress profile due to redistribution of stresses with increasing plasticity and concomitant strain hardening is illustrated in Fig. 14.

CONCLUDING REMARKS

For the first time a complete two-dimensional elastoplastic boundary element formulation has been presented for anisotropic materials. A realistic phenomenological criterion has been adopted to model the yielding and hardening of fiber-reinforced composites.

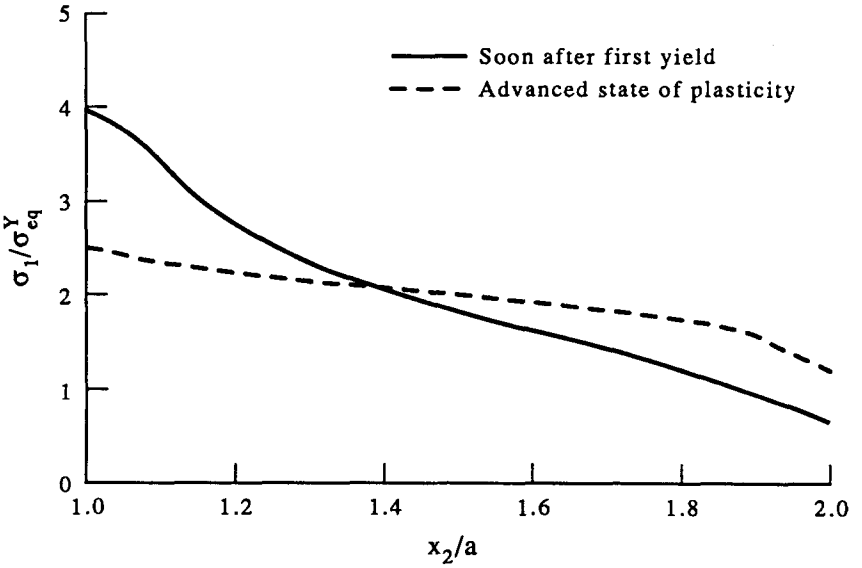

Fig. 14. Comparison of stress profiles at two stages of plasticity.

A new generation Newton–Raphson algorithm has been employed to iteratively solve the nonlinear boundary element equations with a high degree of precision. The boundary element formulation is itself quite general and is not limited by the type of constitutive model used. Thus more general criteria like the Tsai–Wu criterion can easily be incorporated provided adequate and reliable strength parameters are available to justify the use of such a criterion. Numerical validation of the present formulation has been established. The entire procedure is now present in a general-purpose boundary analysis package named GPBEST.

REFERENCES

Banerjee, P. K., Cathie, D. N. and Davies, T. G. (1979). Two and three dimensional problems of elastoplasticity. In *Developments in Boundary Element Methods I* (Edited by P. K. Banerjee and R. Butterfield), Chap. IV, pp. 65–95. Applied Science, Barking.

Banerjee, P. K., Henry, D. P. and Raveendra, S. T. (1989). Advanced inelastic analysis of solids by the boundary element method. *Int. J. Mech. Sci.* **31**(4), 309–322.

Banerjee, P. K. and Butterfield, R. (1981). *Boundary Element Methods in Engineering Science*. McGraw-Hill, Maidenhead.

Banerjee, P. K. and Raveendra, S. T. (1986). Advanced boundary element analysis of two- and three-dimensional problems of elastoplasticity. *Int. J. Numer. Meth. Engng* **23**, 985–1002.

Banerjee, P. K. and Raveendra, S. T. (1987). New boundary element formulation for 2-D elastoplastic analysis. *J. Engng Mech. ASCE* **113**, 252–265.

Cathie, D. N. and Banerjee, P. K. (1980). Boundary element methods in axisymmetric plasticity. In *Innovative Numerical Analysis for the Applied Engineering Sciences* (Edited by R. P. Shaw, D. Pilkey, R. Wilson, A. Lakis, A. Chaduouet and C. Marino). University of Virginia Press, VA.

Chopra, M. B. (1991). Advanced applications of BEM and FEM to axisymmetric nonlinear analysis. Ph.D. dissertation, State University of New York at Buffalo, Buffalo, U.S.A.

Chopra, M. B. and Dargush, G. F. (1992). A Newton–Raphson BEM algorithm for elasto-plasticity. Dept. of Civil Engineering, State University of N.Y. at Buffalo.

Cruse, T. A. and Polch, E. Z. (1986a). Elastoplastic BIE analysis of cracked plates and related problems. Part 1: Formulation. *Int. J. Number. Meth. Engng* **23**(3), 429–437.

Cruse, T. A. and Polch, E. Z. (1986b). Elastoplastic BIE analysis of cracked plates and related problems. Part 2: Numerical results. *Int. J. Numer. Meth. Engng* **23**(3), 439–452.

Deb, A. and Banerjee, P. K. (1990). BEM for general anisotropic 2D elasticity using particular integrals. *Comm. Appl. Numer. Meth.* **6**, 111–119.

Deb, A., Henry, D. P. and Wilson, R. B. (1991). Alternate BEM formulations for 2- and 3-D anisotropic thermoelasticity. *Int. J. Solids Structures* **27**(13), 1721–1738.

Henry, Jr, D. P. and Banerjee, P. K. (1987). A thermoplastic BEM analysis for substructured axisymmetric bodies. *J. Engng Mech. Div. ASCE* **113**, 1880–1900.

Henry, Jr, D. P. and Banerjee, P. K. (1988). A variable stiffness type boundary element formulation for axisymmetric elastoplastic media. *Int. J. Numer. Meth. Engng* **26**, 1005–1027.

Kenaga, D., Doyle, D. F. and Sun, C. T. (1987). The characterization of B/Al composite in the nonlinear range as an orthotropic elastic–plastic material. *J. Composite Materials* **21**, 516–531.

Mukherjee, S. (1982). *Boundary Element Methods in Creep and Fracture*. Elsevier Applied Science, London and New York.

Riccardella, P. (1973). An implementation of the boundary integral technique for planar problems of elasticity and elastoplasticity. Ph.D. thesis, Carnegie Mellon University, Pittsburgh, U.S.A.

Rizzo, F. J. and Shippy, D. J. (1968). A formulation and solution procedure for the general non-homogeneous elastic inclusion problem. *Int. J. Solids Structures* **4**, 1161–1179.

Tsai, S. W. and Wu, E. M. (1971). A general theory of strength for anisotropic materials. *J. Composite Materials* **5**, 58–80.

Watson, J. O. (1979). Advanced implementation of the boundary element method for two- and three-dimensional elastostatics. In *Developments in Boundary Element Methods—1*. (Edited by P. K. Banerjee and R. Butterfield), pp. 31–63. Applied Science Publishers, London.

APPENDIX

Let the angle θ be as defined in Fig. 1 measured in a counter-clockwise direction. The transformation matrix **T** in eqn (11) for 2D analysis is defined as follows:

$$\mathbf{T} = \begin{bmatrix} \cos^2\theta & \sin^2\theta & 2\sin\theta\cos\theta \\ \sin^2\theta & \cos^2\theta & -2\sin\theta\cos\theta \\ -\sin\theta\cos\theta & \sin\theta\cos\theta & \cos^2\theta - \sin^2\theta \end{bmatrix}.$$